Complex martensitic nanostructure in Zr nanowires: A molecular dynamics study

Alexander Thompson and Alejandro Strachan
School of Materials Engineering and Birck Nanotechnology Center, Purdue University, West Lafayette, Indiana 47907, USA
(Received 17 February 2009; revised manuscript received 31 May 2009; published 22 February 2010)

We use molecular dynamics to characterize the martensitic nanostructure that develops when bcc Zr nanowires are cooled down and transform to hcp (martensite). We find that size has a strong effect on nanostructure and even very small wires (a few nanometers in diameter) exhibit complex, multidomain structures with large internal strains (up to ~6%). Long and thin wires result in domains coexisting along their axes while those with small aspect ratios exhibit coexistence of domains within their cross-section. We also that find regions of fcc Zr that develop to bridge neighboring hcp domains.

DOI: 10.1103/PhysRevB.81.085429 PACS number(s): 61.46.Km, 64.70.Nd, 81.30.Kf

I. INTRODUCTION

Understanding size effects in materials behavior and harnessing the phenomena that arises at the nanoscale to achieve improved performance and functionality are significant challenges facing many areas of science and engineering. There is significant interest in the characterization of size effects in optoelectronic,[1] thermal,[2] and mechanical[3] properties, chemical reactivity[4] as well as phase transitions.[5] While significant progress is still required in all these areas solid-to-solid phase transitions is one of the least understood despite its technological importance and recent progress.[6–8] Among such transitions, martensitic ones are particularly interesting since they play a key role in steels[9] and the shape memory effect.[10] In both these examples of martensitic phase transformations the transition from the high-temperature austenite phase to the low-temperature martensite results in a complex microstructure (a variety of domains with different orientations).[11] The resulting microstructures play a critical role in the performance of the martensite and consequently we expect strong size effects when the size of the specimen is reduced below the characteristic length scale of the microstructure. This is critical to assess the possible existence of a limit in miniaturization of NiTi-based shape memory materials. The NiTi martensite phase has been found to be metastable by *ab initio* calculations and the stable ground-state structure is unable to exhibit shape memory; it was proposed that the observed maternsitic structure is stabilized by the internal stresses that result from the microstructure.[12] In this paper we use molecular dynamics (MD) to characterize the martensitic nanostructure in nanoscale Zr wires (nanowires) when the austenite phase (bcc) transforms into martensite (hcp) upon cooling. We find complex, multidomains nanostructures with large internal strains even in nanoscale wires and characterize how such structure is affected by size.

During the bcc to hcp phase transformation a (110) bcc plane transforms into the closed packed plane of the hcp phase; consequently six different hcp variants can be formed from a single bcc crystal. Previous MD simulations on Zr samples with three-dimensional periodic boundary conditions[13] showed that for relative small samples (~10 nm on the side) two or three hcp variants form during quenching. These domains arrange in a twinned structure and inhibited the appearance of others. The authors also found the temporary formation of small fcc domains during the early stages of nanostructure formation; these fcc regions disappear during ripening.

In this paper we characterize the nanoscale polycrystalline structure that develops in Zr nanowires using MD with the same potential employed in Ref. 13: an embedded atom model interatomic potential[14] parameterized to describe the relative energy of various structures, the elastic properties and c/a ratio of the hcp phase and vacancy and stacking faults formation energies. The interatomic potential accurately predicts a transition between bcc and hcp upon cooling as well as twin boundary energies.

II. SIMULATION DETAILS

A. Initial nanowire structures and boundary conditions

The initial structures of our simulations consist of [111] oriented bcc Zr nanowires with circular cross-sections and of various radii and periodic lengths. This orientation leads to low-energy wires in the bcc phase since six closed packed (110) planes are available to form free surfaces. Periodic boundary conditions are imposed in the axial direction of each wire and open boundary conditions are applied in the directions normal to it. In real applications nanowires can experience a variety of boundary conditions in their axial and radial directions depending on growth or fabrication procedure, environment, and other factors. Nanowires grown on a substrate or nanopillars obtained by focused ion beam[3] will have one end interacting (with varying strength) with the substrate while the other end will be free; freestanding wires will have two free ends; and wires bridging two surfaces will experience constrains on both ends. Furthermore, an oxide layer can provide additional constraints in the radial direction. End effects, thus, depend strongly on the fabrication procedure, operation conditions, and environment. While such boundary effects can play an important role in the martensitic transformation for specific applications, the goal of this paper is to identify and characterize general aspects and trends of size effects in martensitic nanostructure and consequently we adopt simple and computationally convenient boundary conditions. In the radial direction we use open boundaries and consider perfectly clean Zr surfaces (no passivation). The periodic boundary conditions we impose in the

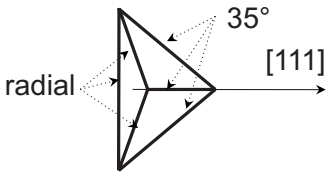

FIG. 1. Orientation of the six possible ⟨110⟩ directions relative the wire axis; each ⟨110⟩bcc can result in a different hcp domain.

axial direction amount to no end effects along the axis of the wires but limit the periodicity of any fluctuation or structure that can develop along this direction to values smaller or equal to the simulation cell length. Periodic boundary conditions are extensively used in atomistic simulations, see for example Ref. 8, but do not represent an experimental configuration. The influence of such boundary conditions on microstructure will be discussed in Sec. IV.

In order to characterize the role of size on martensitic nanostructure we simulated wires with radii varying from 1.6 to 4.5 nm and periodic lengths ranging from 1.6 to 74.6 nm with a total number of atoms up to 191 178.

B. Cooling procedure and domain analysis

We characterize the martensitic nanostructure that develops as temperature is gradually decreased from T=1450 to 300 K in 25 K decrements every 40 ps; temperature is controlled using a Nose-Hoover thermostat[15] and the stress along the wire axis is kept at zero using a Parrinello-Rahman barostat.[16] This cooling rate is typical of MD simulations, see for example Refs. 8 and 13, but very large compared with experiments (even though extremely large cooling rate may be achievable in nanowires due to the large surface to volume ratio). To investigate the sensitivity of our results to cooling rate we performed several simulations with a cooling rate four times higher (25 K every 10 ps) and observe similar trends; the results shown in the remainder of the paper correspond to the slower cooling rate except when explicitly noted otherwise.

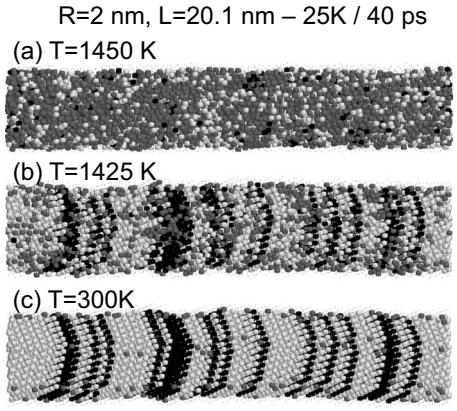

FIG. 2. Atomic structures corresponding to various temperatures for a wire with R=2 nm and L=20.1 nm cooled down by 25 K steps every 40 ps. Light gray represents hcp atoms, dark gray defective ones and black fcc; surface atoms are shown as small dots.

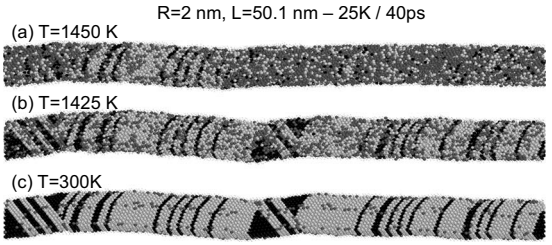

FIG. 3. Atomic structures corresponding to various temperatures for a wire with R=2 nm and L=50.1 nm cooled down by 25 K steps every 40 ps. A multidomain structure develops with fcc regions (black spheres) separating hcp domains.

We analyze the local bonding environment of each atom in terms of the number of first nearest neighbors and the angles between every pair of bonds to characterize the local environment of each atom. Atoms are classified into four categories: (i) hcp, (ii) fcc, (iii) surface [less than 11 nearest neighbors (nn)], and (iv) defective (11 and 13 nn, as well as those with 12 nn that cannot be classified as fcc or hcp based on their bond angles).

III. NANOSTRUCTURE DEVELOPMENT AND CHARACTERISTICS

Figure 1 shows the orientation of the six possible martensite domains relative to the wires axes; we show the six $\langle 110\rangle_{bcc}$ directions which correspond to the possible normals to the closed-packed planes in the hcp structure. Three of these $\langle 110\rangle_{bcc}$ directions are orthogonal to the wire axis and the resulting domains will be denoted *radial*, the remaining three domain normals make an angle of 35.26° with the axis and will be dubbed 35° domains.

Figures 2–7 below show atomic snapshots of our simulations corresponding wires of different geometry during the cooling process and correspond to our slower cooling rate (40 K/25 ps) except for Fig. 5 where results from simulations with faster cooling rate are shown to exemplify the role of cooling rate. In all snapshots throughout the paper gray spheres denote hcp atoms while black ones denote fcc (which often represent stacking faults in the hcp phase); dark gray spheres denote defective atoms and surface atoms are shown as small dots. As will be seen below the transformation starts early in the cooling process, this is in agreement

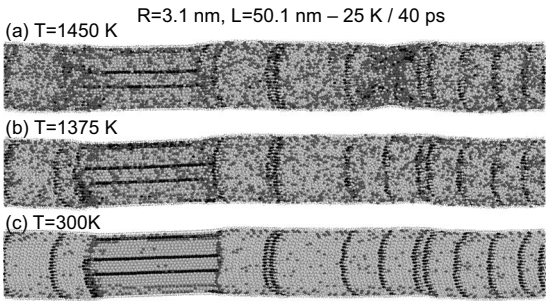

FIG. 4. Atomic structures corresponding to various temperatures for a wire with R=3.1 nm and L=50.1 nm cooled down by 25 K steps every 40 ps.

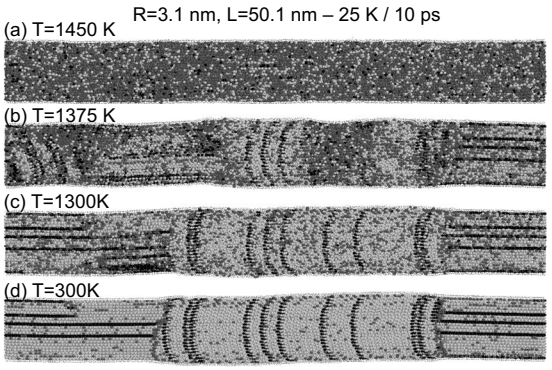

FIG. 5. Atomic structures corresponding to various temperatures for a wire with R=3.1 nm and L=50.1 nm cooled down at a rate faster than that in Fig. 4 by 25 K steps every 10 ps.

with previous work using the same potential;[13] also as was observed upon cooling iron wires in Ref. 8 we do not find a strong size dependence of the transition temperature.

A. Small wires with single-domain structures

The snapshots in Fig. 2 correspond to a wire with initial (bcc at T=1450 K) radius of R=2 nm and periodic length R=20.1 nm and upon cooling it develops a single-domain structure. The orientation of the staking faults in the hcp phase (a planar defect parallel to the closed packed planes with atoms in an fcc local environment and shown as black spheres) enables an easy identification and classification of individual domains. For the wire in Fig. 2 we observe a single 35° domain. We also see that while the wire remains in the bcc phase at T=1450 K the transformation has taken place at T=1425 K, the nanostructure is essentially locked at this high temperature and it remains invariant for the remaining 1,850 ps of the cooling procedure. This indicates that, as expected, stacking faults in hcp have a very low mobility. The geometrical characteristics that tend to lead to single domain structures will be discussed below.

B. Domain coexistence in the axial direction

If the periodic length of the wire is increased to 50.1 nm keeping the radius at R=2 nm we find multiple 35° domains coexisting along the longitudinal direction with no radial domains, Fig. 3. In this case one of the domains is visible at T=1450 K, Fig. 3(a), and the final nanostructure develops at T=1425 K, Fig. 3(b). It is interesting to note that neighboring domains are not simply separated by domain walls but also by wedge-shaped fcc regions. fcc (a metastable phase for Zr) having four {111} (close packed) planes can seamlessly connect to two different hcp domains aligning a $\{111\}_{fcc}$ plane with each of the hcp basal planes (the hcp structure has only one such close packed plane). The angle between the $[110]_{bcc}$ directions that lead to 35° domains is 60° in the austenite phase while the angle between two [111] directions in fcc is ~70.53° so the hcp domains must rotate to accommodate the new structure. This leads to bending of the wire in each interface by an angle of about 10° when measured in the plane containing the two normal to the closed packed plane. This nanostructure is also invariant during over 1.8 ns of cooling from T=1425 to 300 K indicating that the fcc regions that separate hcp domains are very stable and have low mobility.

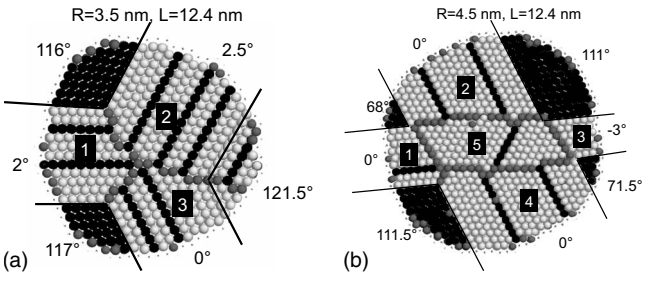

FIG. 6. Cross-sectional microstructure for wires of periodic length L=12.4 nm and two different radii: (a) R=3.5 nm and (b) R=4.5 nm. Note fcc regions (black) bridging between hcp domains.

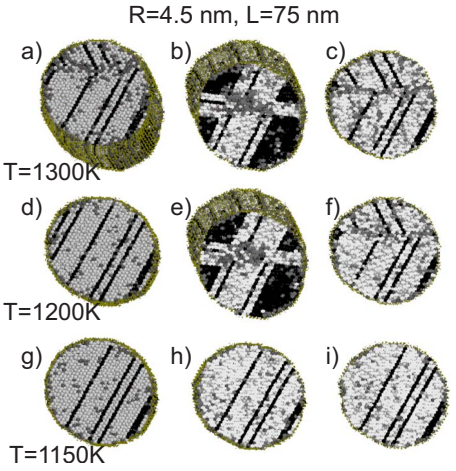

FIG. 7. (Color online) Martensite nanostructure development in a wire with radius 4.5 and periodic length 75 nm. Snapshots correspond to T=1300 K (a)–(c), T=1200 K (d)–(f), T=1150 K (g)–(i), and for each temperature we show three locations along the wire axis.

As the radius of the wire is increased, the nanostructure changes. Figure 4 shows a wire with R=3.1 nm and periodic length L=50.1 nm where we observe the coexistence of both radial and 35° domains; the radial domains can be identified by stacking faults that intersect the wire surface in lines parallel to the wire's axis. These domains are separated by domain walls and not fcc regions. As in the cases described before, the final nanostructure develops at high temperature and is very stable in our simulations. Figure 5 shows the nanostructure development for a wire of the same size as that in Fig. 4 (R=3.1 nm and L=50.1 nm) but cooled down at a higher rate (25 K steps every 10 ps). We see that the final nanostructure has the same characteristics as that of the wire cooled more slowly (coexistence of radial and 35° domains in the axial direction). It is interesting to note that at T=1375 K two radial and two 35° domains can be observed [Fig. 5(b)] but the left most 35° domain disappears during cooling at the two radial domains merge, see snapshot at T=1300 K in Fig. 5(c). Vestiges of the high-temperature

radial domain can be found in the T=300 K structure with a stacking fault ending at the location of the high-temperature interface between the domains.

C. Domain coexistence with the wires cross-section

Multiple domains often coexist within the wire's cross-section in small aspect ratio cases. Figure 6(a) shows the cross-section of a wire with R=3.5 nm and periodic L =12.4 nm that developed the three possible radial domain (marked 1, 2, and 3 in the figure). While a domain wall (gray atoms) separates domains 2 and 3, fcc regions bridge between domains 1 and 2 as well as 1 and 3. As in the case shown in Fig. 3, each fcc section connects two hcp domains arranging two of its {111} planes parallel to the closed-packed plane of each hcp domain and avoiding (partially in this case) a domain wall. Both domain walls and fcc regions are defects in hcp Zr and form to accommodate the various domains that develop during the phase transition. However, fcc atoms have the same coordination number as hcp ones and have lower energy that those in domain walls (with coordination number different from 12). Thus, fcc regions develop to reduce the number of domain wall atoms and minimize the free energy of the system. However, two factors limit the number of fcc regions within a cross-section: geometrical constrains and elastic strain. Consider the angles between rows of atoms in hcp closed-packed planes in each domain, black lines in Fig. 6(a). Ideally, the angle between rows of atoms in neighboring domains would be 120° (this is the angle between the radial $\langle 110 \rangle_{bcc}$ directions and three such domains would close the circle) and rows within the same domain would be parallel to each other. However, the angle between two [111] directions in fcc is only 109.47° and consequently significant internal strain develops to accommodate the observed structure. This is confirmed by the measured angles between atomic rows shown in Fig. 6(a). The $\langle 111 \rangle$ directions in the fcc regions form an angle of 116–117° corresponding of a shear strain of about 6% and two of the hcp regions exhibit a shear strain of about 2%. The presence of a third fcc region in the interface between domains 2 and 3 in the wire shown in Fig. 6(a) would require an angle of 121.5° between its two {111} planes (much larger than the ideal one of 109.47°) leading to even higher internal strains such a pattern was not observed in our simulations. Consequently, the pattern of one domain wall and two fcc regions (or a very similar one) is found in all wires that exhibit three radial domains. Figure 6(b) shows the coexistence of nanoscale domains within a cross-section of a wire with larger radius (R=4.5 nm). The increased size enables a larger number of domains (5 radial hcp ones and 4 fcc) also with fcc regions joining hcp domains. The increased number of domains provides additional flexibility to minimize elastic strains; in this case the strain in the fcc regions is reduced to ~1.5% (from about 6% in the smaller wire) and all but the smallest hcp regions are essentially strain free. Reducing sample size to the nanoscale is generally believed to result in a reduction in the density of defects due to increase importance of free surfaces; however Fig. 6 shows the somewhat surprising results that reducing the cross-sectional size of the wires result in larger internal stresses. It should be pointed out that the periodic boundary conditions imposed on the axial direction of the wires could have an important effect on the nanostructure of small aspect ratio nanowires; additional simulations with open boundary conditions can be expected to yield additional information for these geometries.

D. Single domain structures in larger wires

The snapshots in Fig. 7 depicts the nanostructure development in a wire with R=4.5 nm and L=75 nm (the largest one we studied) for a cooling rate of 25 K/40 ps. Each row shows the cross-sectional nanostructure at three different axial locations corresponding to a given temperature. The initial structure that develops (see T=1300 K snapshots) varies along the axis of the wire; in the central region [Fig. 7(b)] we observe a structure with nine domains similar to that in Fig. 6(b). This structure is surrounded by a two-domain one [Figs. 7(a) and 7(c)] with a domain wall that comes very close to the free surface at one point, Fig. 7(a). As expected, the domain wall moves toward the surface during the annealing process and the structure coarsens to a single domain one at that location as the temperature is reduced to 1200 K [Fig. 7(d)]. Finally, the resulting low-energy, single-domain structure grows in the axial direction and at T=1150 K a single domain runs throughout the whole wire. It is interesting to note that the single domain structure results from the relative long wire periodic length. Increasing the wire's periodic length increases the probability of having a single domain region or one with a structure that can easily evolve toward a single domain [as in Fig. 7(a)]. Once a low-energy, single-domain structure forms in one location it can propagate throughout the wire as long as it is separated from other domains by mobile defects like domain walls.

IV. ROLE OF SIZE ON MARTENSITE NANOSTRUCTURE AND DISCUSSION

To better understand the role of geometry on nanostructure Fig. 8 maps the observed nanostructure as a function of the radius and periodic length of the wires for our slower cooling rate of 25 K per 40 ps. We find a strong correlation between wire geometry and the resulting martensite nanostructure. We can group the behavior in three main categories: (i) long wires exhibit a multidomain structure in which domains coexist along the axis; (ii) for wires with large radii various radial domains coexist within the wires cross-section (thin films would be obtained in the limit of large radii); (iii) both regions of multidomain structures are separated by one involving single-domain wires. We find that the critical radius beyond which multiple radial domains is observed increases rapidly with increasing wire periodic length (note log scale in periodic length); for wires longer than about 50 nm we observe multiple domains along the wire axis.

Two aspects of our simulations can affect the results in Fig. 8 and are worth discussing further: cooling rate and axial boundary conditions. As exemplified in Figs. 4 and 5 increasing the cooling rate by a factor of four to 25 K every

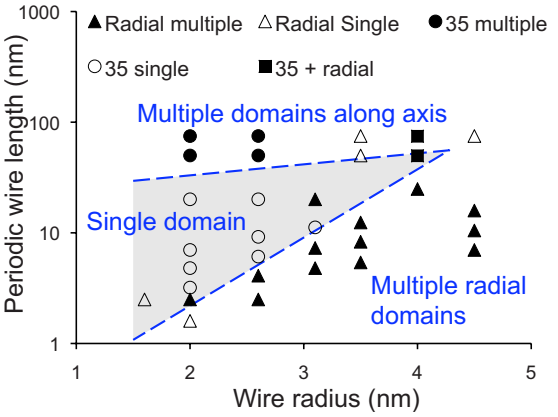

FIG. 8. (Color online) Maps of martensite nanostructure as a function of wire radius and periodic length. We identify three regions: (i) long wires exhibit domain coexistence along their axes, (ii) wires with small aspect ratios exhibit various domains within a cross-section, and (iii) the multidomain regions are separated by a single domain one.

10 ps does not have a strong effect on nanostructure and the trends in Fig. 8 are also valid for the faster cooling. Additional work would be required to assess how significantly slower cooling rates would affect the nanostructure map in Fig. 8; however, due to the low mobility of some of the interfaces between domains we expect the trends observed to remain valid. The second aspect is the dependence of the predicted nanostructure on the wire's periodic length: since this boundary condition does not represent a physical configuration its effects on nanostructure should be carefully analyzed. Axial boundary conditions will affect wires with short lengths more strongly and we expect the nanostructure wires with high aspect ratios to be rather insensitive to boundary conditions. Our simulations show a transition from a single to multiple domains in the axial direction as the periodic length is increased. We expect this general trend to remain valid for other boundary conditions; however, the characteristic length at which the transition occurs is likely to depend on the actual boundary, e.g., free-standing wires or wires/substrate configurations. We expect axial boundary conditions to affect the bottom of Fig. 8 and additional simulations should be performed to further characterize their role on nanostructure.

A comparison of our results with those from previous MD simulations[13] performed with the same interatomic potential and similar cooling rates but periodic boundary conditions in all three directions enables to unambiguously identify nanostructural features that originate from the dimensionality of our systems. Key differences are:

(i) fcc regions to connect neighboring hcp regions are ubiquitous in nanowires and not observed in the equilibrium structure of the three-dimensional (3D) periodic samples;

(ii) nanowires exhibit a significant amount of internal strain even for small radii;

(iii) nanowires exhibit a wide variety of nanostructures depending on their size while only two- or three-domain twinned structures are observed in the 3D periodic case;

V. CONCLUSIONS

In summary, MD simulations show that complex martensitic nanostructures develop in Zr wires even when their size is reduced to the nanoscale. We find very large internal strains, especially for wires of radius close to the threshold associated with multiple domains within a cross-section. We also find several nanostructures that involve a significant fraction of fcc atoms, these regions serve as bridges between hcp domains and replace domain walls. This is a nanoscale phenomenon and we expect fcc domains to play a decreasingly important role as the characteristic size of the nano/microstructure increases; the fcc regions are three dimensional and the number of atoms in them will increase faster than those in two-dimensional domain walls. Our results indicate the possibility of multidomain martensite phases with large internal strains even for nanoscale specimens, opening up the possibility of shape memory at those scales.[12] Detailed information regarding the role of size and geometry on martensitic nanostructure for materials that exhibit shape memory is critical to design nanoscale active materials for applications in MEMS and NEMS and nanostructure maps like that in Fig. 8 could prove to be extremely useful.

ACKNOWLEDGMENTS

This work was partially supported by the U.S. Department of Energy Basic Energy Sciences (DoE-BES) program under program number DE-FG02-07ER46399 (Program Manager: John Vetrano). This work was partially supported by Purdue University and the Network for Computational Nanotechnology through nanoHUB.org computational resources funded by the U.S. National Science Foundation Grant No. EEC-0228390.

[1] Y. Li, F. Qian, J. Xiang, and C. Lieber, Mater. Today **9**, 18 (2006).
[2] Z. H. Wang, J. A. Carter, A. Lagutchev, Y. K. Koh, N. H. Seong, D. G. Cahill, and D. D. Dlott, Science **317**, 787 (2007).
[3] M. Uchic, D. Dimiduk, J. Florando, and W. Nix, Science **305**, 986 (2004).
[4] V. I. Levitas, B. W. Asay, S. F. Son, and M. Pantoya, J. Appl. Phys. **101**, 083524 (2007).
[5] J. Junquera and P. Ghosez, Nature (London) **422**, 506 (2003).
[6] V. A. Lobodyuk, Phys. Met. Metallogr. **99**, 143 (2005).
[7] M. Bouville and R. Ahluwalia, Acta Mater. **56**, 3558 (2008).
[8] L. Sandoval and H. M. Urbassek, Nano Lett. **9**, 2290 (2009).
[9] Keith Bowman, *Mechanical Behavior of Materials* (Wiley, New York, 2004).
[10] Kaushik Bhattacharya, *Microstructure of Martensite* (Oxford University Press, Oxford, UK, 2003).

[11] M. Bouville and R. Ahluwalia, Phys. Rev. Lett. **97**, 055701 (2006).
[12] X. Huang, G. J. Ackland, and K. M. Rabe, Nature Mater. **2**, 307 (2003).
[13] U. Pinsook and G. J. Ackland, Phys. Rev. B **58**, 11252 (1998).
[14] G. Ackland, S. Wooding, and D. Bacon, Philos. Mag. A **71**, 553 (1995).
[15] W. G. Hoover, Phys. Rev. A **31**, 1695 (1985).
[16] M. Parrinello and A. Rahman, J. Appl. Phys. **52**, 7182 (1981); S. Melchionna, G. Ciccotti, and B. L. Hollian, Mol. Phys. **78**, 533 (1993).